Research Article | Vol. 29, No. 19 / 13 Sep 2021 / Optics Express 30694
Optics EXPRESS

Geometric control of vector vortex light beams via a linear coupling system

GUOHUA LIU,[1,2] SHENHE FU,[1,2,3,4] XILIANG ZHANG,[1,2] HAO YIN,[1,2,3] ZHEN LI,[1,2,3,5] AND ZHENQIANG CHEN[1,2,3]

[1]Department of Optoelectronic Engineering, Jinan University, Guangzhou 510632, China
[2]Guangdong Provincial Key Laboratory of Optical Fiber Sensing and Communications, Guangzhou, 510632, China
[3]Guangdong Provincial Engineering Research Center of Crystal and Laser Technology, Guangzhou 510632, China
[4]fushenhe@jnu.edu.cn
[5]ailz@126.com

Abstract: We demonstrate a novel theoretical platform to realize geometric control of vector vortex states in an optical coupling system. These complex states are characterized by spatially varying polarizations and coupled with vortex phase profiles. It can be mapped uniquely as a point on a higher-order Poincaré sphere. The geometric theory clearly reveals how a tailored phase mismatch profile, together with a suitable coupling, supports state conversion between these higher-order complex light fields, in analogous to the processes appearing in two-level quantum system as well as three-wave mixing process in nonlinear optics. Specifically, in the phase matching condition, it is shown that these complex states carried by an envelope field exhibit periodic oscillations in the course of state evolution; whereas in the phase mismatching condition the oscillations become detuned, leading to noncyclic state evolution. Intriguingly, when using an adiabatic technique for the phase mismatch, robust state conversion between two arbitrary vector vortex light fields can be realized. Our demonstrations provide a fully control over the vector vortex states on the sphere, and we suggest that it would benefit various potential applications both in the classical and the quantum optics.

1. Introduction

The state of polarization of light is related to its vectorial nature of electromagnetic filed. It has became one of the most salient features of the light field [1]. The polarization state in the scalar regime, such as the state containing homogeneous linear, circular, or elliptic polarization, is associated with the spin angular momentum and therefore it can be mapped as a point on the conventional spin-based Poincaré sphere [2]. Such a geometric description relies on orthogonal basis of two pure spin states (i.e., the left and the right circular polarizations) mapped on the north and south poles of the sphere, respectively [3]. When the orthogonal spin basis is endowed with the orbital angular momentum of light, it constructs a spin-orbit based Poincaré sphere, also called as the higher-order Poincaré sphere [4,5]. A linear combination of these spin-orbit bases results in vector vortex state, which exhibits inhomogeneous polarization distributions in transverse plane and are featured by helical wave front characterized by a topological charge [4,5]. It is worth mentioning that the state of polarization of the higher-order vector vortex beam can also be geometrically described as a point on the surface of the higher-order sphere, in a similar way to that shown by the conventional Poincaré sphere. Among them, the two pure states mapped on the poles of the sphere degrade into homogeneous circular polarizations having vortex phase profiles, while the equator characterizes vector beam with inhomogeneous linear polarizations. Other points between the poles and equator exhibit vector states of elliptical polarizations. It is emphasized that these higher-order vector vortex states are solutions to the vectorial Maxwell

#435152 https://doi.org/10.1364/OE.435152
Journal © 2021 Received 24 Jun 2021; revised 30 Aug 2021; accepted 31 Aug 2021; published 8 Sep 2021

Optics EXPRESS

wave equation [1,6], and can be experimentally realized by many techniques implemented both inside [7,8] or outside [9,10] the laser cavities. This geometric representation provides not only deep insight into the light field, but also greatly simplifies problems of description for the complex polarizations.

In recent years, the vector vortex beams have been widely studied in various aspects owing to their intriguing spin-orbit coupling properties of the light fields [11–14]. For example, a specific type of vector vortex state undergoes an adiabatic transformation through an anisotropic medium where the intrinsic spin and orbital components evolve in a particular way, resulting in the spin-orbit Hall effect of light [15]. Manifestations of spin-orbit interactions of the vector vortex beams have been reported as spin state splitting on the Poincaré sphere, accompanied with vectorial spin Hall effect of light [16]. When tightly focusing the vector vortex light beam, a strong longitudinal polarization of light field can be achieved [17], accompanied by a phenomenon of spin-to-orbital angular momentum conversion [14]. In addition to these intriguing classical properties, the vector vortex light beam has also been applied to quantum regime [18,19], where the vector vortex beam can be possible to encode unlimited quantum states with discrete topological charges.

Despite great potential shown by the vector vortex light beams, to date, on-demand controlled conversion between such complex states is not achieved. We note that several attempts have been made to structure design that allows vector vortex state conversions between specific points on the higher-order sphere [11,15,20]. Nevertheless, each conversion requires its own design, and no theory so far has been developed to account for the spin-orbit coupling dynamic of the vector vortex state in the course of state conversion.

In this article, we come up with and demonstrate a novel theoretical platform to realize geometrical control of the vector vortex state of light fields via a linear coupling system. We take advantage of analogies between the Poincaré sphere and the Bloch sphere that is used for describing quantum state dynamics in two-level system [21,22], as well as the three-wave mixing process in nonlinear optics [23]. In this regard, we built the connection between these different settings, and present, for the first time, a geometric theory that clearly reveals how a tailored phase mismatching quantity, together with a suitable coupling strength, supports robust state conversion between these complex vector vortex light beams.

2. Principle for the geometric control

A very powerful method to represent polarization state is the Poincaré sphere. This sphere maps the complex Jones vectors into points on this sphere, where the north and south poles represent two orthotropic states of polarizations. This concept of geometric representation was later adopted for representing other types of dynamic two-level systems, including spins in magnetic field [24], as well as atomic two-level system coupled by electromagnetic waves [21,25], and is known in quantum mechanics as the Bloch sphere. As shown in Fig. 1(a), the quantum state in a two-level quantum system can be described by a Bloch sphere, expressed as $\vec{\rho} = (U, V, W)$ [21]. On the sphere, the south and north poles represent the two orthogonal eigenstates of the two-level system, i.e., the ground state $|w_g>$ and the excited state $|w_e>$, as marked in the Fig. 1(a). The quantum wave packet evolves according to an action of an external electromagnetic field. The mechanism for driving the evolution process of the quantum state is that the two pure states become interactive with each other under the driving of external field. The coupling effect can be mapped onto a form of the torque vector $\vec{g}$, as is illustrated in the figure. Therefore, the state evolution on the Bloch sphere can be geometrically controlled by the torque vector $\vec{g}$, which is associated with the external field and their detuning. In this case, the dynamics of the quantum system satisfies the classical gyro equation [22], represented by the precession of the state around the torque vector $\vec{g}$, as is illustrated in Fig. 1(a).

Optics EXPRESS

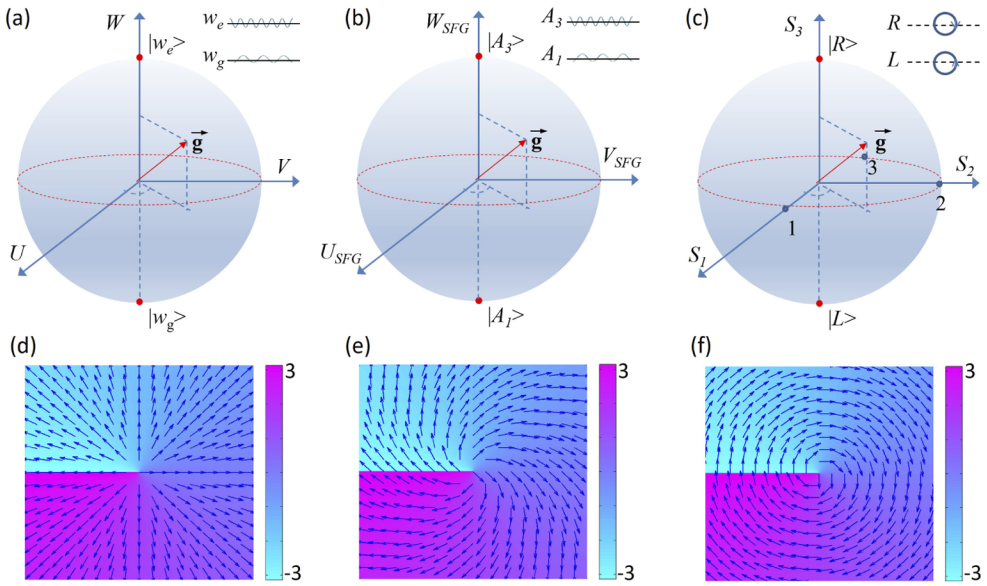

Fig. 1. Principle for geometric control of wave packets in different physical settings: (a) The Bloch sphere describing quantum states in the two-level quantum systems. The pure states denoted by $|\omega_g>$ and $|\omega_e>$ are mapped on the south and north poles of the sphere. The state evolves according to the rotation of the torque vector $\vec{g}$. (b) The Bloch sphere representing three-wave mixing process in $\chi^{(2)}$ nonlinear optics. The idler $|A_1>$ and signal $|A_3>$ waves represent the two orthotropic pure states, while the pump wave $|A_2>$ drives the nonlinear process, as a result, the nonlinear state $\vec{\rho} = (U_{SFG}, V_{SFG}, W_{SFG})$ rotates according to the torque vector $\vec{g}$. Here SFG denotes the process of sum-frequency generation. (c) Higher-order Poincaré sphere ($\ell = 1$) used to map the vector vortex states. The two pure sates are represented by the left $|L>$ and $|R>$ circularly polarized vortex beams. In an analogous manner, the state $\vec{S} = (S_1, S_2, S_3)$ evolves according the the torque vector $\vec{g}$. (d)-(f) Representations of typical vector vortex states mapped on the equator of the sphere, see the points marked as 1, 2, 3 in (c), respectively.

An equivalent of a spinor has been recently shown in nonlinear optics. The optical structure with $\chi^{(2)}$ nonlinearity couple the idler $|A_1>$, signal $|A_3>$ and pump waves $|A_2>$. In this three-wave mixing process, the idler and the signal waves represent the spin down and spin up equivalents [26], as depicted, respectively, on the south and north poles of the Bloch sphere, see Fig. 1(b); while the pump wave acts as an external field that drives the nonlinear process. Particularly note that, a geometric representation for the nonlinear three-wave mixing process was already developed [23,26]. In that scenario, all possible nonlinear light states can be shown on the surface of a Bloch sphere constructed by the three components of a state vector $\vec{\rho}_{SFG} = (U_{SFG}, V_{SFG}, W_{SFG})$, which are related to the idler and the signal waves. Note that here SFG denotes the sum-frequency generation. This representation is closely connected to the description of the vector vortex states on the higher-order Poincaré sphere, and it generates fully optical manipulations for the idler and signal waves, hence leading to novel nonlinear phenomena. For instance, the light-matter interactions in a modulated $\chi^{(2)}$ nonlinear crystal have led to notable outcomes including the recent finding of a new form of geometric phase [27–29], the all-optical Stern-Gerlach effect [26], and the optical skyminons (a topological texture of spin distribution) [30].

We explore the underlying SU(2) structure of the higher-order Poincaré sphere, compared to that discussed in the two-level quantum settings [21,25] as well as nonlinear optics [23,26]. We define a higher-order poincaré sphere constructed by three Stokes parameters, represented

Optics EXPRESS

by S_1, S_2, and S_3, respectively, as illustrated in Fig. 1(c). On the Poincaré sphere, the north and south poles of the sphere represent two orthogonal eigenmodes, corresponding to the left ($|L>$) and right ($|R>$) circularly-polarized vortex light fields. Note that these two eigenmodes have opposite topological charges $\pm\ell$. As mentioned, the vector vortex state mapped at other point on the sphere is a linear combination of the two eigenstates. For instance, we present three typical mixed states mapped on the equator of the sphere, see the points marked as 1, 2, 3 on the equator, corresponding to an azimulthal angle of 0, $\pi/2$, and π. Their corresponding polarization distributions are illustrated in Fig. 1(d), 1(e) and 1(f), respectively. In order to geometrically control the vector vortex states on the sphere, it is required to couple the two orthogonal polarized light modes in an optical system, in an analogous way to the two-level system as well as the three-wave mixing process. In this work, the coupling effect between two orthotropic polarization components could take place in a single-mode anisotropic fiber [31], where these two modes exhibit different refringence index, let's say n_x and n_y, respectively, while having the same transverse profile during propagation. The birefringence effect of the fiber structure gives rise to different group velocities of the two components. As a result, phase mismatching appears in the course of beam propagation, which in turn affects the dynamics of the vector vortex state. This effect plays a role of 'external field' that drives the motion of the vector vortex state on the sphere. It can be predicted that the coupling effect and the phase mismatching quantity can be mapped into an analogous torque vector $\vec{g}$, which determines the evolution process of the vector vortex state.

3. Theoretical model

Any state of polarization of the complex vector vortex light fields can be represented as a form of superposition of two antipodal circular polarization basis [4,5]

$$\Psi = [cos(\frac{\theta}{2})\exp(-i\frac{\phi}{2})]|\hat{L}>+[\sin(\frac{\theta}{2})\exp(i\frac{\phi}{2})]|\hat{R}>, \tag{1}$$

where $|\hat{R}> = \exp(+i\ell\varphi)(\hat{x} - i\hat{y})/\sqrt{2}$ and $|\hat{L}> = \exp(-i\ell\varphi)(\hat{x} + i\hat{y})/\sqrt{2}$ represents right- and left-circularly polarized vortex beams with topological charge of ℓ and $-\ell$, respectively. $\hat{x}$ and $\hat{y}$ are unitary vectors indicating polarizations along x and y coordinates, respectively, and $\varphi = \arctan(y/x)$. i is the imaginary unit. Evidently, these two pure states $|R>$ and $|L>$ exhibit homogenous polarization distributions and are coupled by the reciprocal vortex phase. Note that ϕ and θ denote, respectively, the azimuthal and polar angles in the Poincaré sphere for which the geometrical coordinates are represented by three Stokes parameters: S_1 , S_2 and S_3, as illustrated in Fig. 1(c) [it shows the first-order ($\ell = 1$) Poincaré sphere]. We express the vector vortex state as $\Psi(\varphi) = \Psi_x(\varphi)\hat{x} + \Psi_y(\varphi)\hat{y}$, where

$$\begin{aligned}\Psi_x(\varphi) &= \kappa_1 \exp(-i\ell\varphi) + \kappa_2 \exp(+i\ell\varphi),\\ \Psi_y(\varphi) &= i\kappa_1 \exp(-i\ell\varphi) - i\kappa_2 \exp(+i\ell\varphi).\end{aligned} \tag{2}$$

Here the coefficients κ_1 and κ_2 denote the weights of the left and the right components, respectively, and take the following forms

$$\begin{aligned}\kappa_1 &= \frac{1}{\sqrt{2}}\cos\left(\frac{\theta}{2}\right)\exp\left(-i\frac{\phi}{2}\right),\\ \kappa_2 &= \frac{1}{\sqrt{2}}\sin\left(\frac{\theta}{2}\right)\exp\left(+i\frac{\phi}{2}\right).\end{aligned} \tag{3}$$

A linearly coupled system for the vector vortex states is exploited, in which the two components of the states become coupled during state evolution. As mentioned above, this could be

Optics EXPRESS

implemented possibly through optical birefringent fiber where the state components Ψ_x and Ψ_y undergo different refractive index, leading to different group velocities [31]. Besides, one can also explore possibilities with optical cavities [32], coupled waveguides [33,34], or space-varying birefringent wave plates [20] for coupling the two polarization components. To demonstrate geometric control of the complex light field, we consider a vector vortex state carried by an evolving envelope field $E(x, y, z)$, where z denotes the evolution axis in the setting. In this case, the full vector of the vector vortex light field is expressed as $\mathbf{E} = E(x, y, z)\Psi$. Evolution of state of polarization on the Poincaré sphere can be realized by utilizing a linearly coupled wave equation under the paraxial condition. In the normalized form, it can be written as [31]

$$\begin{aligned} i\frac{\partial E_x}{\partial z} + \frac{\partial^2 E_x}{\partial x^2} + \frac{\partial^2 E_x}{\partial y^2} + CE_y \exp(+i\Delta\beta z) = 0, \\ i\frac{\partial E_y}{\partial z} + \frac{\partial^2 E_y}{\partial x^2} + \frac{\partial^2 E_y}{\partial y^2} + CE_x \exp(-i\Delta\beta z) = 0, \end{aligned} \tag{4}$$

where E_x and E_y represents the Cartesian polarization components of the light field $\mathbf{E}$. C is the mixing strength of these two components. In general, C is a constant and its strength is related to optical power of the light field. Note that the terms $\exp(\pm i\Delta\beta z)$ are the accumulated phase difference between these two components during evolution in the anisotropic fiber, with $\Delta\beta = \beta_x - \beta_y$ being their phase mismatch. It is related to the birefringent effect of the fiber, i.e., $\Delta\beta \propto \Delta n$, where $\Delta n = n_x - n_y$. We assume that the system has no loss, hence the evolution of the complex state along the Poincaré sphere is adiabatic. The theoretical model in Eq. (4) reveals that the phase mismatching quantity $\Delta\beta$ together with a suitable coupling strength C governs the adiabatic evolution of the vector vortex states on the sphere.

We further note that the second and third terms of the coupled wave equations stand for spatial diffraction of the light field, which does not alter the state of polarization during evolution in the system. In general, this terms can be neglected owing to the fact that the light wave propagates in a specific spatial mode which does not change significantly in the course of propagation. Therefore, to look for a geometric representation for the state evolution on the higher-order Poincaré sphere, it is convenient to remove these diffraction terms. As a result, we simplify the coupled wave equation as

$$\begin{aligned} \frac{\partial E_x}{\partial z} &= iCE_y \exp(+i\Delta\beta z), \\ \frac{\partial E_y}{\partial z} &= iCE_x \exp(-i\Delta\beta z). \end{aligned} \tag{5}$$

These simplified wave equations are tantamount to those for geometrical control of the quantum state in the two-level quantum system [21,25]. The populations of the ground and excited states (i.e., ω_g and ω_e) in a quantum setting are analogous to the pure states ($|L>$ and $|R>$) of the sphere in an optical system. Time evolution is replaced by propagation along the z axis, and the detuning $\Delta\omega = \omega_e - \omega_g$ is replaced by the phase-mismatch $\Delta\beta$. Additionally, these coupled wave equation of the vector vortex light field shows analogies to the three-wave mixing process in nonlinear optics, as already demonstrated both theoretically and experimentally [23,26]. These analogies among different systems refer to Fig. 1(a)–1(c). To realize geometric representation for the vector vortex light beams, we recall the Stokes parameters, which are real functions of evolution axis z, and defined as [4,5]

$$\begin{aligned} S_1 &= E_x E_x^* - E_y E_y^*, \\ S_2 &= E_x E_y^* + E_y E_x^*, \\ S_3 &= i(E_x E_y^* - E_y E_x^*), \end{aligned} \tag{6}$$

where $(*)$ indicates complex conjugate. These three parameters satisfy:$S_1^2 + S_2^2 + S_3^2 = S_0^2$, where $S_0 = E_x E_x^* + E_y E_y^*$ denotes the total power of the light field. In a normalized form, it reduces to a

Optics EXPRESS

form of $S_0 = 1$. We adopt these three Stokes parameters to construct a sphere. Note that when $\ell = 0$, the sphere is reduced to a conventional spin-based Poincaré sphere, in which the state of plane wave polarization of a beam is represented, as suggested by the definition of $|R>$ and $|L>$. However, for $\ell \geq 1$, it constructs a spin-orbit-based Poincaré sphere, also known as the higher-order sphere [4,5], where the complex vector vortex state can be mapped uniquely. Here we limit our discussions on the higher-order regime.

We define a state vector, represented by three Stokes parameters, $\vec{S}(z) = (S_1(z), S_2(z), S_3(z))$ whose z dependence can be obtained from the above coupled wave equation. For a given z, the state vector $\vec{S}(z)$ can be represented as a point on the surface of the sphere. For example, taking into account the north and south poles of a normalized sphere, the corresponding state vectors are mapped as $\vec{S} = (0, 0, 1)$ and $\vec{S} = (0, 0, -1)$, respectively. We further deduce the motion equation of the state vector $\vec{S}(z)$, expressed in a form of $d\vec{S}/dz = \vec{g} \times \vec{S}$, where $\vec{g} = (g_1, g_2, g_3)$ is a torque vector. Three components of $\vec{g}$ are obtained as $g_1 = 0$, $g_2 = -2C\cos(\Delta\beta \cdot z)$, and $g_3 = 2C\sin(\Delta\beta \cdot z)$, respectively. Clearly, the torque vector $\vec{g}$ represents the coupling between the two fields. Note that the symbol $\times$ denotes the vector product. The picture resembles the geometric descriptions for other settings, as illustrated in Fig. 1(c), showing the precession of the vector vortex state around the torque vector $\vec{g}$. The explicit form of the underlying three-wave coupling equation for the vector $\vec{S}(z)$ can be written as

$$\begin{aligned} \frac{dS_1}{dz} &= -2C\cos(\Delta\beta \cdot z)S_3 - 2C\sin(\Delta\beta \cdot z)S_2, \\ \frac{dS_2}{dz} &= 2C\sin(\Delta\beta \cdot z)S_1, \\ \frac{dS_3}{dz} &= 2C\cos(\Delta\beta \cdot z)S_1. \end{aligned} \tag{7}$$

This dynamic problem is nontrivial and can be solved with the initial (boundary) conditions, represented by: $S_1(0) = \sin(\theta)\cos(\phi)$, $S_2(0) = \sin(\theta)\sin(\phi)$, and $S_3(0) = \cos(\theta)$, respectively. In general, the complex dynamic problem of the vector vortex fields can be simplified when the phase of the two orthotropic components are matched, i.e., $\Delta\beta = 0$. Analytic solution can be also found, as already demonstrated in the context of light-matter interaction in the two-level systems, as well as nonlinear optics. However, in most cases where the phase mismatch becomes non-zero or variant with state evolution, it is difficult to obtain its analytical solution. In the following, we will utilize this model to demonstrate numerically adiabatic state conversion between the vector vortex light beams.

4. Adiabatic conversions between vector vortex states

Firstly, we examine the situation of $\Delta\beta = 0$, also called as a perfect phase matching condition. This resembles the resonant condition of the two-level quantum states. In this case, full conversion of the initial vector vortex state to another state is achievable. The perfect-phase-matched solution for the vector vortex state exhibits similar dynamical features as those reported in resonant condition of the two-level physical settings. This results in periodic evolution of the vector vortex state, as visualized in the Poincaré sphere as a periodic rotation of the state vector $\vec{S}$ started form the point: $\vec{S} = (1, 0, 0)$, see the red circle on the sphere in Fig. 2(a). This phenomenon is known as the Rabi oscillation, which was already investigated extensively in the quantum physics [35–40], but it is rarely studied with the vector vortex light beams. Here we demonstrate the Rabi oscillation of light waves in the framework of higher-order vector vortex regime. This new oscillating states of light are characterized by a topologically shaped wavefront and coupled by spatially varying polarization. Figure 2(b) shows the corresponding variation of the three stokes components along with the propagation distance. It is clearly seen that the components of S_1 and S_3 exhibit harmonic oscillation following a sin or cos function but with different phase offsets,

Optics EXPRESS

a phenomenon of Rabi oscillation. Contrary to S_1 and S_3, the value of S_2 shows no variation during state evolution on the Poincaré sphere. This is because the derivative of the second wave equation in Eq. (7) becomes zero and hence it is independent on the value of S_1 and S_3. To further observe this intriguing 'Rabi oscillation', we simulate propagation of the vector vortex beams based on Eq. (4), by means of the numerical method of the 4th Runge-Kutta. To this end, we take into account the light field which contains vortex phase with topological charge of $|\ell| = 1$. The vector vortex state is carried by an envelope having the Laguerrre-Gauss profile. In this scenario, the initial condition for the Eq. (4) takes the following form

$$\mathbf{E}(r, z = 0) = r \cdot \exp\left(-\frac{r^2}{\sigma_0^2}\right)\left[\Psi_x(\varphi)\hat{x} + \Psi_y(\varphi)\hat{y}\right], \tag{8}$$

where $r = (x^2 + y^2)^{1/2}$, and σ_0 denotes the Gaussian waist that is set as $\sigma_0 = 15$ in the following discussions. By setting the initial state vector: $\vec{S}(z = 0) = (1, 0, 0)$, i.e., the evolution process of the vector vortex state starts from a mixed state mapped on the equator of the sphere, expressed as $(\theta, \phi) = (\pi/2, 0)$, we obtain vector vortex state conversion along a periodic trajectory on the sphere, with outcomes depicted in Fig. 2(d). The states at different points are characterized by the x-components of the vector vortex light fields. At the beginning, the $x-$component shown in the first panel of Fig. 2(d) indicates a vector vortex state having radial polarization distribution. Owing to the spin-orbit coupling in the anisotropic structure that rotates the torque vector $\vec{g}$ on the sphere, the state gradually converts into another states having elliptical polarization, see the panel 2 and the corresponding point on the sphere. After a quarter of a cycle, the state evolves into a pure state having homogeneous circular polarization and coupled with vortex phase with topological charge of $\ell = 1$, see the panel 3. In this case, the x-component of the light field shows a doughnut shaped profile in the transverse plane. After half a circle of evolution, the state becomes azimuthally polarized, as suggested from the panel 5. Afterwards, the reverse evolution process begins and the vector vortex state evolves gradually back to its origin, as illustrated in the panels 6-8 in Fig. 2(d). These results show direction observation of the Rabi oscillation of the vector vortex light fields. The new optical oscillating state is different from previously reported Rabi oscillation of the wave [35–40]. It is featured by a topological wave front and coupled by the spatially varying polarization. Furthermore, we show that the vector vortex state also exhibits analogous cyclic conversion with another initial state marked as $(\theta, \phi) = (\pi/2, \pi/4)$, with result shown by the blue trajectory in Fig. 2(a). Different from the red trajectory on the sphere, the state starts with a more complex phase distribution with local polarization angle of $\pi/4$. But similar effect of circle oscillation of the state can be observed. The real-time evolution of the Stokes parameters further indicate its periodic oscillation, as shown in Fig. 2(c). It is clearly seen that the evolution process follows the same periodic function, except for that the values of S_2 in these two cases are different. These results suggest that the Rabi frequency in the phase matching condition is independent to the initial states.

Next, we consider the case where the phase of the two orthotropic components of the complex light field are mismatched in the course of propagation. In this 'non-resonant' condition, the setting does not support complete cycle conversion between two target states, since all components of the state vector $\vec{S}$ become coupled, as indicated by the theoretical model in Eq. (7). As a result, the value of each Stokes component is a function of distance z and is related to $\Delta\beta$. To see this detuned effect, we take the value of $\Delta\beta = 2.5$ into account, and set the initial state located at the equator of the sphere, expressed as $(\theta, \phi) = (\pi/2, 0)$. With these settings, we obtain the evolution trajectory mapped on the Poincaré sphere, as illustrated by the blue curve in Fig. 3(a). Distinctive features can be indicated: first, the evolution trajectory becomes noncyclic and flopping around the initial point of the sphere; second, the detuning effect leads to a relatively low oscillating amplitude of S_1 around a specific value. This phenomenon is further confirmed by the real-time value of the Stokes parameters, as illustrated in Fig. 3(b). On the other hand, we consider another

Optics EXPRESS

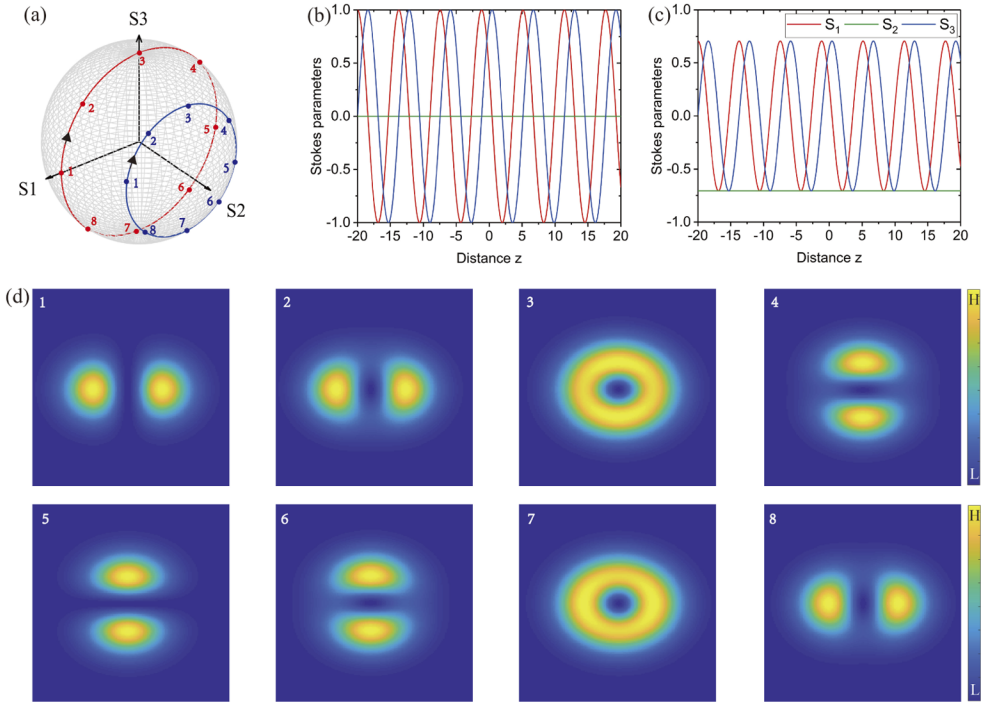

Fig. 2. Periodic evolution of the vector vortex states represented by the first-order Poincaré sphere, under the setting: $\Delta\beta = 0$, and $C = 1$. (a) Geometrical visualization of the state evolution on a sphere. Two periodic trajectories are plotted for different initial states, expressed as: $(\theta, \phi) = (\pi/2, 0)$ (see the red curve), and $(\theta, \phi) = (\pi/2, \pi/4)$ (see the blue curve). (b) and (c) present their corresponding variations of the Stokes parameters along with the evolution. (d) Direct observation of the periodic conversion of the vector vortex light beams, based on the model in Eq. (4). The panels denote intensity distributions of x-components of the light fields at different points of the sphere, see the red curve in (a). In the color bars, L: Low; H: High.

process where the state starts from another point on the sphere, expressed as $(\theta, \phi) = (\pi/2, -\pi)$. This vector vortex state exhibits π-phase shift as compared to the initial state depicted by the process (see the blue curves). Interestingly, it is shown from the Stokes parameters [see Fig. 3(c)] that the value of the Stokes parameter is also π-phase shifted for the same detuning, as compared to the results in Fig. 3(b). The outcome for this process is presented in Fig. 3(a), see the red trajectory on the sphere. It is shown that the two initial π-symmetric states (z=0) exhibit similar behaviors in the course of their evolutions, as suggested from the resultant evolution trajectories both having flower patterns on the sphere.

It is worth noting that both the phase matching and mismatching conditions give rise to oscillations of the vector vortex states when given an input state. These instable state conversion of the vector vortex light field hinders its potential applications. For example, to achieve conversion between two target states, one should carefully design an anisotropic structure with delicate detuning and interaction length. Slight difference would lead to a failure conversion of the vector vortex states. In the following, we investigate possibilities for robust conversion between two arbitrary vector vortex states, by means of an adiabatic technique. In this case, the phase mismatching quantity $\Delta\beta$ is no longer a constant. It should vary adiabatically along the propagation distance. It means that the refractive index of n_x and n_y is no longer independent of propagation distance, but it is subject to a corresponding modulation function of z. The adiabatic

Optics EXPRESS

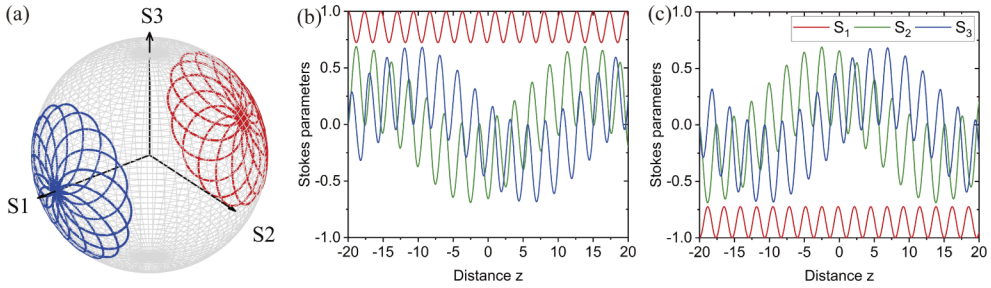

Fig. 3. Non-periodic evolution of the vector vortex states represented by the first-order Poincaré sphere, under the setting: $\Delta\beta = 2.5$, and $C = 1$. (a) Geometric evolution trajectories of the vector vortex states starting from different initial points: $(\theta, \phi) = (\pi/2, 0)$ (see the blue curve), and $(\theta, \phi) = (\pi/2, \pi)$ (see the red curve). (b) and (c) present their corresponding variations of the Stokes parameters along with the evolutions.

process can be realized by sweeping the rate of the phase mismatch along the z axis, so that it changes slowly with respect to the adiabatic condition [41]

$$\left| C \cdot \frac{d\Delta\beta}{dz} \right| \ll \left(C^2 + \Delta\beta^2 \right)^{\frac{3}{2}}. \tag{9}$$

This adiabatic profile of the $\Delta\beta$ can be realized possibly by setting the phase mismatch following a nonlinearly chirped function, written as:

$$\Delta\beta(z) = \beta_0 \tanh(\gamma_1 \cdot z + \gamma_2 \cdot z^2 + \gamma_3 \cdot z^3), \tag{10}$$

where β_0 is an offset of the phase, and γ_j $(j = 1, 2, 3)$ is coefficient that controls the sweeping rate of the phase mismatch. We should point out that one could also exploit other types of modulated functions for the $\Delta\beta(z)$, not limited to the case we utilized here, as long as they satisfy the adiabatic condition. According to the modulation model, we can achieve robust conversions between two arbitrary vector vortex states. Without loss of generality, let's consider the adiabatic process where a mixed state is converted into another mixed state on the sphere. To this end, we perform numerical analysis based on the theoretical model in Eq. (5), taking into account the settings: $C = 1$, $\beta_0 = 115.2$ and $\vec{S}(z = 0) = (1, 0, 0)$. Note that the inhomogeneous polarization distribution of the initial state is shown in the Fig. 1(d). Figure 4(a) illustrates clearly the conversion process: at the beginning, owing to the large phase mismatch β_0, the torque vector $\vec{g}$ does not move significantly and cycles in the vicinity of the initial point. As a result, the vector vortex state exhibits weakly evolution around the initial point of the sphere. With the evolution, the sweeping rate of the phase mismatch changes adiabatically from negative to positive values. In this case, the state evolves accordingly into the target mixed state with polarization distribution depicted in Fig. 1(f). The geometric trajectory of the adiabatic process can be seen from the surface of the Poincaré sphere as shown in Fig. 4(a). We monitor the variation of the Stokes parameters with propagation distance, with result presented in Fig. 4(a1). It is shown, indeed, that the value of state vector $\vec{S} = (1, 0, 0)$ remains unchanged at the early state of evolution, and then it transfers adiabatically into the desired state ($\vec{S} = (-1, 0, 0)$) with a very short coupling length scale. Afterwards, the converted state becomes stable, as seen from the invariant value of $\vec{S}$ at the final stage of evolution. To further confirm this robust conversion process, numerical observations are also presented, based on the model in Eq. (4). Figure 4(a2) shows the outcomes, showing the x-component of the light field before and after the conversion. It is seen that the horizontal component at the beginning exhibits two symmetric main lobes along the x coordinates; whereas the horizontal component rotates by an angle of $\pi/2$ at the final stage of evolution, suggesting a state conversion during the light wave propagation.

Optics EXPRESS

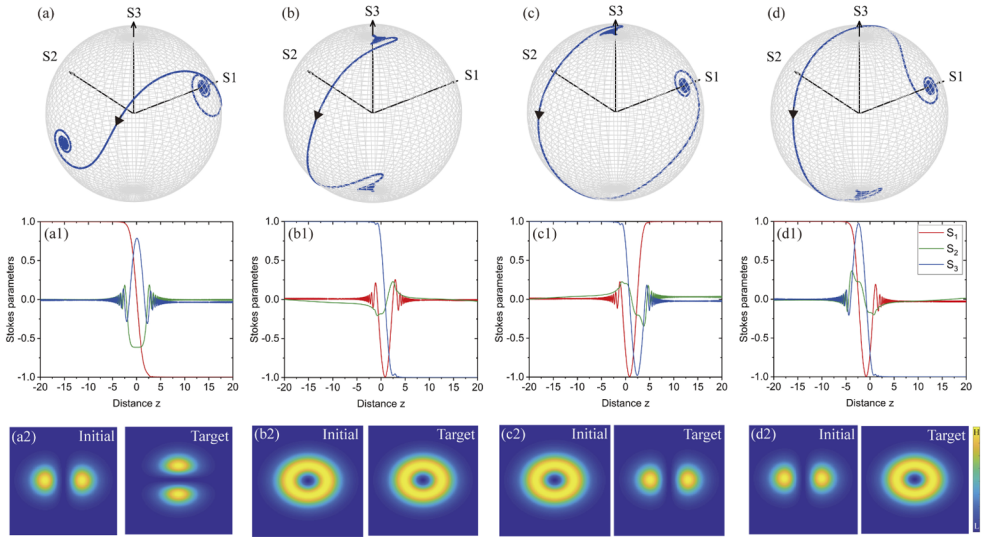

Fig. 4. Robust conversion between two arbitrary vector vortex light states by means of the adiabatic technique. Without loss of generality, four different types of conversion processes are presented based on the first-order Poincaré sphere: (a) mixed state→mixed state, i.e., $(\pi/2, 0)$→$(\pi/2, \pi)$; (b) pure state→pure state, i.e., it starts from the north pole and ends by the south pole; (c) pure state→mixed state, i.e., it starts from the north pole, and ends at a point at $(\pi/2, 0)$; and (d) mixed state→pure state, i.e., it starts from a point $(\pi/2, 0)$ and ends at the south pole. (a1)-(d1) The corresponding variations of the Stokes parameters along with state evolutions, obtained from the model in Eq. (7); whereas (a2)-(d2) show the intensity distributions of x-components of the initial and targets states, corresponding to the processes in (a)-(d). Note that the simulations were performed based on Eq. (4), under the settings: $C = 1$, $\beta_0 = 115.2$, and (a, a1, a2) $\gamma_1 = -2.00 \times 10^{-4}$, $\gamma_2 = 2.04 \times 10^{-4}$, and $\gamma_3 = -6.10 \times 10^{-4}$; (b, b1, b2) $\gamma_1 = -55.10 \times 10^{-4}$, $\gamma_2 = 42.86 \times 10^{-4}$, and $\gamma_3 = -10.20 \times 10^{-4}$; (c, c1, c2) $\gamma_1 = 59.18 \times 10^{-4}$, $\gamma_2 = -38.80 \times 10^{-4}$, and $\gamma_3 = 6.12 \times 10^{-4}$; (d, d1, d2) $\gamma_1 = 59.18 \times 10^{-4}$, $\gamma_2 = 38.78 \times 10^{-4}$, and $\gamma_3 = 6.12 \times 10^{-4}$.

To further demonstrate the availability of the technique, we consider other different processes. We classify them into three types of conversion processes: the pure state to pure state, the pure state to mixed state, and the mixed state to pure state, corresponding to the results as illustrated in Fig. 4(b, b1, b2), Fig. 4(c, c1, c2), and Fig. 4(d, d1, d2), respectively. We should note that these different conversion processes are implemented under the same settings, but with different values of γ_j, as specified in the caption of Fig. 4. As seem from their evolution trajectories on the sphere, all the considered states exhibit slightly evolutions on the sphere at their early stages, owing to the large mismatch. Afterwards, they evolve into their target states adiabatically and finally become stable. Such an evolution feature is further indicated by their corresponding value of $\vec{S}$. As direct evidence, we also present intensity distributions of the horizontal components of the fields at the beginning and final stages of state evolution, see the corresponding results in Fig. 4(b2)–4(d2), respectively. These results suggest that using the adiabatic technique, we can realize robust conversion between two arbitrary vector vortex states.

5. Conclusion

In conclusion, we have demonstrated a novel geometric technique for controlling the state of polarization of light in the framework of a spin-orbit based Poincaré sphere. Coupled wave theory was adopted to account for the spin-orbit coupling dynamics of the complex light field in

Optics EXPRESS

the setting, which plays a role in a manner similar to the two-level quantum system [21,25], as well as three-wave mixing process in nonlinear optics [23,26]. We have shown the intriguing Rabi oscillating properties of the vector vortex state in the phase matching condition. Such an effect of Rabi oscillation takes place in the framework of the higher-order optical regime, hence it contrasts to previously demonstrated Rabi oscillations [35–40]. On the other hand, we have considered the behaviors of vector vortex state in the phase mismatching condition, featuring by the nonclyclic evolution process. This detuned effect leads to inefficient state conversion of the light field. Importantly, in order to obtain a robust and high efficient conversion between two target complex states, adiabatic technique was utilized for tailoring the phase mismatch profile. In this regards, we have demonstrated four different types of adiabatic conversion processes, including conversion from any mixed state to mixed state of the light field. We believe our demonstrations open new possibilities for control and manipulation of the vector vortex light fields, and might find intriguing applications both in the quantum and the classical optics [42,43]. This works would also trigger new studies of the spin-orbit properties of light, accompanied by the evolution processes.

Funding. National Natural Science Foundation of China (11974146, 62175091); Special Project for Research and Development in Key areas of Guangdong Province (2020B090922006); Guangzhou Municipal Science and Technology Project (201904010094); Science and Technology Planning Project of Guangdong Province (2018B010114002); the Pearl River talent project (2017GC010280).

Disclosures. The authors declare no conflicts of interest.

Data availability. Data underlying the results presented in this paper are not publicly available at this time but may be obtained from the authors upon reasonable request.

References

1. Q. Zhan, "Cylindrical vector beams: from mathematical conceopts to applications," Adv. Opt. Photonics **1**(1), 1–57 (2009).
2. S. M. Barnett, L. Allen, R. P. Cameron, C. R. Gilson, M. J. Padgett, F. C. Speirits, and A. M. Yao, "On the natures of the spin and orbital parts of optical angular momentum," J. Opt. **18**(6), 064004 (2016).
3. M. Born and E. Wolf, *Principles of Optics*, 7th ed. (Cambridge University, 1999).
4. G. Milione, H. I. Sztul, D. A. Nolan, and R. R. Alfano, "Higher-Order Poincaré Sphere, Stokes Parameters, and the Angular Momentum of Light," Phys. Rev. Lett. **107**(5), 053601 (2011).
5. G. Milione, S. Evans, D. A. Nolan, and R. R. Alfano, "Higher Order Pancharatnam-Berry Phase and the Angular Momentum of Light," Phys. Rev. Lett. **108**(19), 190401 (2012).
6. D. G. Hall, "Vector-beam solutions of Maxwell's wave equation," Opt. Lett. **21**(1), 9–11 (1996).
7. D. Naidoo, F. S. Roux, A. Dudley, I. Litvin, B. Piccirillo, L. Marrucci, and A. Forbes, "Controlled generation of higher-order Poincaré Sphere beams from a laser," Nat. Photonics **10**(5), 327–332 (2016).
8. K. Yan, J. Lin, Y. Zhou, C. Gu, L. Xu, A. Wang, P. Yao, and Q. Zhan, "Bi_2Te_3 based passively Q-switched fiber laser with cylindrical vector beam emission," Appl. Opt. **55**(11), 3026–3029 (2016).
9. X. Wang, J. Ding, W. Ni, C. Guo, and H. Wang, "Generation of arbitrary vector beams with a spatial light modulator and a common path interferometric arrangement," Opt. Lett. **32**(24), 3549–3551 (2007).
10. S. Chen, X. Zhou, Y. Liu, X. Ling, H. Luo, and S. Wen, "Generation of arbitrary cylindrical vector beams on the higher order Poincaré Sphere," Opt. Lett. **39**(18), 5274–5279 (2014).
11. R. C. Devlin, A. Ambrosio, N. A. Rubin, J. P. B. Mueller, and F. Capasso, "Arbitrary spin-to-orbital angular momentum converison of light," Science **358**(6365), 896–901 (2017).
12. F. Bouchard, H. Larocque, A. M. Yao, C. Travis, I. De Leon, A. Rubano, E. Karimi, G. Oppo, and R. W. Boyd, "Polarization Shaping for Control of Nonlinear Propagation," Phys. Rev. Lett. **117**(23), 233903 (2016).
13. C. Guo, S. Fu, H. Lin, Z. Li, H. Yin, and Z. Chen, "Dynamic control of cylindrical vector beams via anisotropy," Opt. Express **26**(14), 18721–18733 (2018).
14. P. Yu, Y. Liu, Z. Wang, Y. Li, and L. Gong, "Interplay between Spin and Orbital Angular Momenta in Tightly Focused Higher-Order Poincaré Sphere Beams," Ann. Phys. **532**(8), 2000110 (2020).
15. S. Fu, C. Guo, G. Liu, Y. Li, H. Yin, Z. Li, and Z. Chen, "Spin-Orbit Optical Hall Effect," Phys. Rev. Lett. **123**(24), 243904 (2019).
16. W. Zhu, H. Zheng, Y. Zhong, J. Yu, and Z. Chen, "Wave-Vector-Varying Pancharatnam-Berry Phase Photonic Spin Hall Effect," Phys. Rev. Lett. **126**(8), 083901 (2021).
17. H. Wang, L. Shi, B. Lukyanchuk, C. Sheppard, and C. T. Chong, "Creation of a needle of longitudinally polarized light in vacuum using binary optics," Nat. Photonics **2**(8), 501–505 (2008).

Optics EXPRESS

18. D. Cozzolino, E. Polino, M. Valeri, G. Carvacho, D. Bacco, N. Spagnolo, L. K. K. Oxenløwe, and F. Sciarrino, "Air-core fiber distribution of hybrid vector vortex-polarization entangled states," Adv. Photonics **1**(4), 046005 (2019).
19. A. Sit, F. Bouchard, R. Fickler, J. Gagnon-Bischoff, H. Larocque, K. Heshami, D. Elser, C. Peuntinger, K. Günthner, B. Heim, C. Marquardt, G. Leuchs, R. W. Boyd, and E. Karimi, "High-dimensional intracity quantum cryptography with structured photons," Optica **4**(9), 1006–1010 (2017).
20. W. Shu, X. Ling, X. Fu, Y. Liu, Y. Ke, and H. Luo, "Polarization evolution of vector beams generated by q-plates," Photonics Res. **5**(2), 64–72 (2017).
21. L. D. Allen and J. H. Eberly, *Optical Resonance and Two Level Atoms* (Wiley, 1975).
22. R. P. Feynman, F. L. Vernon, and R. W. Hellwarth, "Geometrical Representation of the Schrödinger Equation for Solving Maser Problems," J. Appl. Phys. **28**(1), 49–52 (1957).
23. H. Suchowski, D. Oron, A. Arie, and Y. Silberberg, "Geometrical representation of sum frequency generation and adiabatic frequency conversion," Phys. Rev. A **78**(6), 063821 (2008).
24. I. I. Rabi, "Space Quantization in a Gyrating Magnetic Field," Phys. Rev. **51**(8), 652–654 (1937).
25. J. J. Sakurai and J. Napolitano, *Modern Quantum Mechanics*, 2nd ed. (Addison-Wesley, 2011).
26. A. Karnieli and A. Arie, "All-Optical Stern-Gerlach Effect," Phys. Rev. Lett. **120**(5), 053901 (2018).
27. A. Karnieli and A. Arie, "Fully controllable adiabatic geometric phase in nonlinear optics," Opt. Express **26**(4), 4920–4932 (2018).
28. A. Karnieli, S. Trajtenberg-Mills, G. D. Domenico, and A. Arie, "Exprimental observation of the geometric phase in nonlinear frequency conversion," Optica **6**(11), 1401–1405 (2019).
29. Y. Li, O. Yesharim, I. Hurvitz, A. Karnieli, S. Fu, G. Porat, and A. Arie, "Adiabatic geometric phase in fully nonlinear three-wave mixing," Phys. Rev. A **101**(3), 033807 (2020).
30. A. Karnieli, S. Tsesses, G. Bartal, and A. Arie, "Emulating spin transport with nonlinear optics, from high-order skyrmions to the topological Hall effect," Nat. Commun. **12**(1), 1092 (2021).
31. G. P. Agrawal, *Nonlinear Fiber Optics* (Wiely, 2012).
32. D. Colas, L. Dominici, S. Donati, A. A. Pervishko, T. C. H. Liew, I. A. Shelykh, D. Ballarini, M. de Giorgi, A. Bramati, G. Gigli, E. del Valle, F. P. Laussy, A. V. Kavokin, and D. Sanvitto, "Polarization shaping of Poincaré beams by polariton oscillations," Light: Sci. Appl. **4**(11), e350 (2015).
33. Y. Xu, S. Chen, Z. Wang, B. Sun, H. Wan, and Z. Zhang, "Cylindrical vector beam fiber laser with a symmetric two-mode fiber coupler," Photonics Res. **7**(12), 1479–1484 (2019).
34. Y. V. Kartashov, V. A. Vysloukh, and L. Torner, "Resonant mode oscillations in modulated waveguiding structures," Phys. Rev. Lett. **99**(23), 233903 (2007).
35. B. Y. Chang, I. R. Sola, and V. S. Malinovsky, "Anomalous Rabi Osicllations in Multilevel Quantum Systems," Phys. Rev. Lett. **120**(13), 133201 (2018).
36. A. Schülzgen, R. Binder, M. E. Donovan, M. Lindberg, K. Wundke, H. M. Gibbs, G. Khitrova, and N. Peyghambarian, "Direct Observation of Excitonic Rabi Oscillations in Semiconductors," Phys. Rev. Lett. **82**(11), 2346–2349 (1999).
37. Y. V. Bludov, V. V. Konotop, and M. Salerno, "Rabi oscillations of matter-wave solitons in optical lattices," Phys. Rev. A **80**(2), 023623 (2009).
38. Y. O. Dudin, L. Li, F. Bariani, and A. Kuzmich, "Observation of coherent many-body Rabi oscillations," Nat. Phys. **8**(11), 790–794 (2012).
39. F. Assemat, D. Grosso, A. Signoles, A. Facon, I. Dotsenko, S. Haroche, J. M. Raimond, M. Brune, and S. Gleyzes, "Quantum Rabi Osicllation in Coherent and in Mesoscopic Cat Field States," Phys. Rev. Lett. **123**(14), 143605 (2019).
40. M. R. Matthews, B. P. Anderson, P. C. Haljan, D. S. Hall, M. J. Holland, J. E. Williams, C. E. Wieman, and E. A. Cornell, "Watching a Superfluid Untwist Itself: Recurrence of Rabi Oscillations in a Bose-Einstein Condensate," Phys. Rev. Lett. **83**(17), 3358–3361 (1999).
41. H. Suchowski, G. Porat, and A. Arie, "Adiabatic processes in frequency conversion," Laser Photonics Rev. **8**(3), 333–367 (2014).
42. Z. Luo, W. Pang, B. Liu, Y. Li, and B. Malomed, "A new form of liquid matter: Quantum droplets," Front. Phys. **16**(3), 32201 (2021).
43. Y. Shen, X. Wang, Z. Xie, C. Min, X. Fu, Q. Liu, M. Gong, and X. Yuan, "Optical vortices 30 years on: OAM manipulation from topological charge to multiple singularites," Light: Sci. Appl. **8**(1), 90 (2019).